

1 Influence of paste thickness on coated aggregates on properties of
2 high-density sulphoaluminate cement concrete

3 Sun Keke¹, Zhou Xiangming², Gong Chenchen¹, Ding Yanyu¹, Lu
4 Lingchao¹

5
6 1. Shandong Provincial Key Laboratory of Preparation and Measurement of Building
7 Materials, Jinan, Shandong, China, 250022

8 2. Department of Mechanical, Aerospace and Civil Engineering, Brunel University
9 London, Uxbridge, Middlesex UB8 3PH, United Kingdom

10
11 **Abstract:** An improved method for the densified mixture design algorithm and Fuller
12 curve were used to design high-density sulphoaluminate cement concrete (HDSC). The
13 performance of HDSC is significantly influenced by the paste thickness on the coated
14 aggregates. Sulphoaluminate cement concrete mixtures containing aggregates coated
15 with 3 different paste thickness of $t=10\mu\text{m}$, $20\mu\text{m}$, and $30\mu\text{m}$ and water-binder ratios
16 (W/B) of 0.25, 0.30 and 0.35 were prepared. The results of experiments show that
17 paste thickness on the coated aggregates significantly influences the mechanical
18 properties and durability of HDSC. With the increase of paste thickness, the
19 compressive strength is increased, but the electrical resistivity is decreased, particularly
20 at the early ages of 1 and 3 days. The sulfate corrosion resistance coefficients of HDSC
21 are larger than 1.0, the total porosity can be less than 7%, and the micropore (i.e. with
22 pore size less than 20nm) can be larger than 70%.

23 **Keywords:** sulphoaluminate cement concrete; Fuller curve; densified mixture design
24 algorithm; coating thickness; durability

25 **1. Introduction**

26 Sulphoaluminate cement is a type of “low energy” cement compared to Portland
27 cement [1], possessing advantageous properties such as high early-age compressive
28 strength, short setting time and shrinkage compensation and it is typically used in the

29 marine engineering field [2-4]. However, as a special type of cement, the mechanical
30 properties and durability [5-6] of sulphoaluminate cement concrete (SACC) has not
31 been well studied. Under harsh environments, the harmful external ions and water can
32 easily permeate into the concrete interior, destroying its structure and shorten its
33 service life. However, a compact concrete structure can lead to improved strength and
34 durability. The importance of pore structure and its impact on durability has been
35 highlighted in numerous studies [7]. Many researchers also found that the concrete
36 pore structure improved the interfacial transition zone (ITZ) and dominated
37 engineering properties, such as strength and durability [8-9]. For such reasons,
38 high-density concrete has been widely used to achieve outstandingly durable concrete
39 structures.

40 However, it must be noted that little work has been conducted on SACC mixture
41 design as a high-density concrete. Therefore, the major work required is designing an
42 appropriate mix proportion to produce the high-density sulphoaluminate cement
43 concretes (HDSCs). The densified mixture design algorithm (DMDA) is derived from
44 the maximum density theory and excess paste theory, proposed by Hwang et al.
45 [10-12]. This method is based on the hypothesis that the physical properties can be
46 optimized when the packing density is high. The major difference from the other
47 mixture design algorithms is that instead of partial replacement of cement, DMDA
48 incorporated the use of fly ash to fill the void between aggregates and hence increase
49 the density of the aggregate system. In such a way, the cement paste content can be
50 reduced without affecting the other properties such as workability, and strength [13].
51 Lots of research [13-16] shows that it is feasible to produce the eco-friendly
52 construction bricks, lightweight concrete, high-performance concrete and
53 self-compacting concrete using the DMDA method with the incorporation of an
54 admixture, such as fly ash or slag powder. However, to simplify the derivation, it is
55 necessary to assume that the aggregate is spherical, which is physically very hard to
56 achieve and thus gives rise to errors.

57 In additional, it is commonly thought that the cement paste volume is a key factor
58 in achieving a desirable concrete workability and durability [17-19]. A work studied

59 the effect of cement content on transport processes important to the durability of
60 concrete structures, such as electrical conduction and chloride diffusion. It was found
61 that the resistance to transport reduced as cement content was increased [20]. Hwang et
62 al. proposed a particular DMDA, in which the concept and formula of the paste
63 thickness on coated aggregates were introduced. A complete and precise formula to
64 estimate the optimum coating thickness on the aggregates was derived to ensure the
65 use of sufficient coating paste and a dense concrete structure is obtained [21]. Koliass
66 and Georgiou studied the effect of paste volume and of water content on capillary
67 absorption and strength on concrete mixes. It is found that strength increases and
68 capillary absorption decreases when the volume of the water or the volume of the paste
69 decreases [22]. Chen et al. demonstrated that the paste thickness on the coated
70 aggregates has a positive effect on the slump flow, concluding that a thickness of $42\mu\text{m}$
71 produced self-compacting concrete which flowed to a diameter of 680mm [23]. Last
72 but not least, using less cement reduces energy consumption and CO_2 emissions
73 associated with its production process.

74 In this paper, an improved DMDA method is developed to simplify the
75 calculation process. Introducing the assumption that the aggregates are square and
76 spherical in shape allows a more accurate engineering design requirement to prepare
77 HDSC. The Fuller curve was used to calculate the aggregate gradation, and the sieve
78 analysis was used to calculate the specific surface area of aggregates. Sulphoaluminate
79 cement, replaced by approximately 5% superfine slag powder, and 10% fly ash, both
80 by weight, was used as the cementitious materials for preparing the HDSC and the
81 improved DMDA calculated the dosage of cementitious material. Finally, the effects of
82 paste thickness around the aggregates on mechanical and durability properties of
83 HDSC were investigated.

84

85 **2. Raw materials and methods**

86 ***2.1 Sulphoaluminate cement and admixtures***

87 Sulphoaluminate cement of strength class 42.5, fly ash and slag powder were
88 imported from mainland China. The chemical compositions of the sulphoaluminate

89 cement, fly ash and slag powder are shown in Table 1. The average particle size of fly
 90 ash and slag powder are $14.34\mu m$ and $2.98\mu m$, respectively. The superplasticizer (SP)
 91 used was a polycarboxylate polymer, and its water-reducing capacity in SACC was
 92 over 20%.

93 Table 1 Chemical composition of raw materials (wt.%)

Materials	SiO ₂	Al ₂ O ₃	CaO	MgO	Fe ₂ O ₃	Other	Loss
Sulphoaluminate cement	11.41	27.87	43.86	-	2.59	13.11	1.16
Fly ash	50.55	29.01	6.00	5.44	-	4.12	2.08
Slag powder	29.46	17.44	34.71	11.02	-	0.3	0.30

94

95 2.2 Aggregates

96 River sand (0.075-2.36mm in size) was used as fine aggregates with an apparent
 97 density of $2710kg/m^3$, and crushed natural stone (2.36-16mm in size) was applied as a
 98 coarse aggregate with an apparent density of $2740kg/m^3$. The aggregate mix
 99 proportions were also key to improving the packing density of concrete [24]. Fuller
 100 curve was based on defining conventional concrete dosages by selecting coarse and
 101 fine aggregate proportions according to the adjustment within the standard curve that
 102 allows for the maximum compaction of granular elements, which is the method that
 103 corresponds to the Gessner parabola [25]. Since the Fuller curve was proposed, it has
 104 been used for designing concrete mixes for many applications, particularly for those of
 105 high-density and high-performance concrete [26-28]. The Fuller curve is a series of
 106 curves, widely used for the optimization of concrete aggregates, and expressed as:

$$107 \quad U(j) = 100 \times (j/D_{max})^h \quad (1)$$

108 where $U(j)$ is the total volume percent of particles passing through a sieve, (%); D_{max} is
 109 the maximal size of the aggregate, (mm); j is the diameter of the particular sieve, (mm);
 110 and h is the exponent of the equation.

111 The value for h , which varies from 0.33 to 0.45, was selected as 0.33 [26, 29] in
 112 this study. The mass ratios of aggregates of different particle size are given in Table 2,
 113 calculated using Equation (1).

114

Table 2 Mass ratios of aggregates with different gradations (wt.%)

Grain size (mm)	0.075-0.15	0.15-0.30	0.30-0.60	0.6-1.18	1.18-2.36	2.36-4.75	4.75-9.50	9.50-16.0
wt. %	0.13	0.17	0.21	0.27	0.35	0.47	0.43	0.39

115

116 **2.3 Methods**

117 ***2.3.1 Concrete samples preparation***

118 The concrete samples were made according to Chinese national standard for
 119 testing fresh concrete GB/T50080-2002 [30] (equivalent to ASTM C192M-02). All
 120 concrete samples, measured $100\text{mm} \times 100\text{mm} \times 100\text{mm}$, were cured at $20 \pm 2^\circ\text{C}$ in
 121 moulds for the first 24h, then demoulded and cured in an environment of $20 \pm 2^\circ\text{C}$ and
 122 at $95 \pm 5\%$ RH until the day of testing.

123

124 ***2.3.2 Compressive strength test***

125 The compressive strength test of concrete was carried out according to the
 126 Chinese National Standard for testing mechanical properties of concrete GB/T
 127 50081-2002 [31] (equivalent to ASTM C39). The compressive strength of concrete
 128 was evaluated for the ages of 1, 3 and 28 days at a loading rate of 0.5MPa/s as per
 129 GB/T 50081-2002.

130

131 ***2.3.3 Electrical resistance test***

132 In this study, the concrete was mixed with a water-binder ratio (0.25, 0.30 and
 133 0.35) and cast into 100mm^3 cubes for the electrical resistance test. The negative and
 134 positive copper electrodes were placed parallel to each other inside the cubic concrete
 135 samples, and the average testing results of the three samples were taken as the
 136 representative value. The schematic diagram of the concrete specimen prepared for
 137 electrical resistivity measurement is shown in Fig.1.

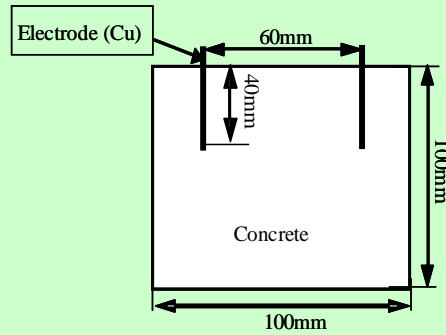


Fig.1 Schematic diagram for concrete electrical resistivity measurement

138
139
140

2.3.4 Sulfate attack resistance

142 The resistance of concrete to sulfate attack was conducted according to Chinese
143 national standard for testing durability of concrete GB/T 50082-2009 [32] (equivalent
144 to ASTM C 1012). The solution was made by dissolving reagent grade sodium sulfate
145 (Na_2SO_4) in deionized water and contained a final SO_4^{2-} concentration of 33,800ppm
146 (i.e. 5% Na_2SO_4). All specimens were stored in plastic containers having the solution
147 with ample space between them. The containers with the specimens were stored in a
148 constant temperature ($20\pm 1^\circ\text{C}$) room and the solutions were replenished periodically
149 once a week to remain the designated concentration. Other control concrete cubes were
150 kept in deionized water as well. The degree of sulfate attack was evaluated by
151 measuring the compressive strength of concrete samples at 28 days, and the ratio of
152 compressive strength was calculated by Equation (2) as follows:

$$153 \quad K_f = \frac{f_{cn}}{f_{c0}} \quad (2)$$

154 where, K_f is the compressive strength ratio, (%); f_{c0} is the average compressive strength
155 (in MPa) of the control concrete cubes cured for 28 days in deionized water; and f_{cn} is
156 the average compressive strength (in MPa) of three concrete cubes immersed in 5%
157 sodium sulfate solution for 28 days.

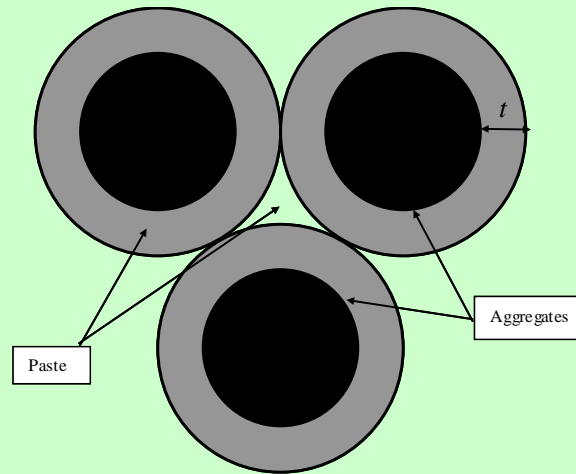
158

3. Dosage of cementitious materials

3.1 Packing model of concrete

161 According to classical concrete mixture proportion design, the aggregates are
162 considered the main skeleton of concrete and the paste requirements for workable

163 concrete are determined by the aggregate gradation. Effective packing can be attained
 164 by selecting accurate proportions of small size particles to fill in the voids between the
 165 bigger particles. The Fuller model is considered to be an effective method for
 166 preparing high-density concrete by adjusting the particle size for optimum aggregate
 167 packing [33-34]. The concrete model structure is shown in Fig.2. In the diagram, the
 168 aggregates, shown in black, are representing the concrete skeleton, the paste coating
 169 them is shown in gray, and the white area among the aggregates are the voids.



170

171

Fig.2 Diagrammatic model of aggregates and paste in concrete.

172

173 **3.2 Calculation process of cement paste dosage**

174 (1) The calculation process of the specific surface area of aggregates

175 The aggregate specific surface area calculation process was simplified by
 176 assuming all aggregates to be either spherical or square. The volume of each particle is
 177 shown in the Equation (3):

$$\begin{array}{l}
 \text{178 Spherical:} \\
 \text{179 Square:}
 \end{array}
 \left.
 \begin{array}{l}
 \frac{m}{\rho} = V = \frac{4}{3}\pi\left(\frac{D}{2}\right)^3 = \frac{1}{6}D \cdot \pi D^2 = \frac{1}{6}D \cdot A \\
 \frac{m}{\rho} = V = D^3 = \frac{1}{6}D \cdot 6D^2 = \frac{1}{6}D \cdot A
 \end{array}
 \right\} \quad (3)$$

180 Then, according to the definition of the specific surface area with the combination
 181 of Equation (3), Equation (4) could be derived as following.

$$\text{182 } \frac{n \cdot A}{n \cdot m} = \frac{A}{D \cdot A \cdot \rho} \cdot 6 = \frac{6}{D \cdot \rho} \quad (4)$$

183 where m is the mass of each aggregate particle, (in g); ρ is the apparent density of
 184 aggregates, (in kg/m^3); V is the volume of each aggregate particle, (in cm^3); D is the
 185 particle size of aggregate, (in mm); A is the specific surface area of each aggregate
 186 particle, (in cm^2); and n is the number of aggregate particles.

187 The aggregate is of varying particle size, so the specific surface area of the
 188 aggregates could be achieved according to Equation (5):

$$189 \quad A_s = \frac{\sum_i \left(\frac{6000}{D_i \cdot \rho} m_i \right)}{M} = \frac{6000}{\rho} \cdot \sum_i \left(\frac{K_i}{D_i} \right) \quad (5)$$

190 where A_s is the specific surface area of aggregates, (in m^2/kg); D_i is the intermediate
 191 particle size of each aggregate gradation, (in mm); M is the total mass of aggregates,
 192 (in kg); m_i is the total mass of each aggregate gradation, (in kg); and K_i is the mass
 193 fraction of each aggregate gradations, i.e. m_i/M in %. Based on calculation, the specific
 194 surface area of aggregates with different gradations is shown in Table 3.

195

Table 3 Specific surface area of aggregates

Gradation (mm)	D_i (mm)	K_i (%)	A_s (m^2/kg)
0.075-0.15	0.11	4.5	
0.15-0.30	0.23	6.0	
0.30-0.60	0.45	7.8	5.73
0.60-1.18	0.92	10.0	
1.18-2.36	1.77	12.7	
2.36-4.75	1.20	17.1	
4.75-9.50	7.13	21.7	0.71
9.50-16.0	12.75	20.4	

196 (2) The calculation process of the total paste volume

197 Supposing that the average paste thickness of coated aggregates was termed as t
 198 (in μm), the dosage of paste was calculated using Equations (6) and (7):

$$199 \quad V = t \cdot (M_s A_s + M_G A_G) + V_b \quad (6)$$

200 where V is the unit volume of the paste, (in m^3); t is the average paste thickness on the
 201 coated aggregates, (in μm); M_s is the dosage of fine aggregates, (in kg); M_G is the
 202 dosage of coarse aggregates, (in kg); A_s is the specific surface area of fine aggregates,
 203 (in m^2/kg); A_G is the specific surface area of coarse aggregates, (in m^2/kg); and V_b is the
 204 volume of paste required to fill the pores between the aggregates, (in m^3);

205
$$V_b = \frac{M_s}{\rho_s} \cdot P_s = \frac{M_s}{\rho_s} \cdot \left(1 - \frac{\rho_s}{\rho'_s}\right) \quad (7)$$

206 where ρ_s is the packing density of fine aggregates, (in kg/m^3); ρ'_s is the apparent
 207 density of fine aggregates, (in kg/m^3); and P_s is the porosity of fine aggregates, (in %).

208 Based on the concept of particle packing, well-graded aggregates have fewer
 209 voids among particles than poorly graded aggregates requiring less cement paste to fill
 210 the voids. Thus, the additional amount of cement paste remaining can be used to coat
 211 the aggregate particles and improve the concrete fluidity. For the same reason, an
 212 increase in the volume fraction of aggregates generally results in a reduced concrete
 213 fluidity. A high-density concrete with desirable workability is obtained when a suitable
 214 amount of cement paste is provided to fill the spaces among the aggregates. The
 215 dosages of cementitious materials with coating thickness of $t=10\mu m$, $20\mu m$ and $30\mu m$
 216 [35-36] are shown in Table 4, respectively. The water-binder ratio was fixed at 0.25,
 217 0.30 and 0.35 after a series of trial mixes, satisfying the requirements of concrete with
 218 a slump of $250\pm 10mm$, respectively.

219 Table 4 Water-binder ratio and dosages of cementitious material in HDSCs

No.	Water-Binder ratio	Coating thickness	Cement (kg/m^3)	FA (kg/m^3)	SS (kg/m^3)	SP (kg/m^3)
A1	0.25	$t=10\mu m$	324	74	39	4.37
B1		$t=20\mu m$	382	88	47	5.17
C1		$t=30\mu m$	441	101	54	5.96
A2	0.30	$t=10\mu m$	299	69	36	4.04
B2		$t=20\mu m$	353	81	43	4.77
C2		$t=30\mu m$	407	94	50	5.51
A3	0.35	$t=10\mu m$	278	64	34	3.76
B3		$t=20\mu m$	328	75	40	4.43
C3		$t=30\mu m$	378	87	46	5.11

220

221 4. Results and Discussions on Properties of HDSC

222 4.1 Compressive strength

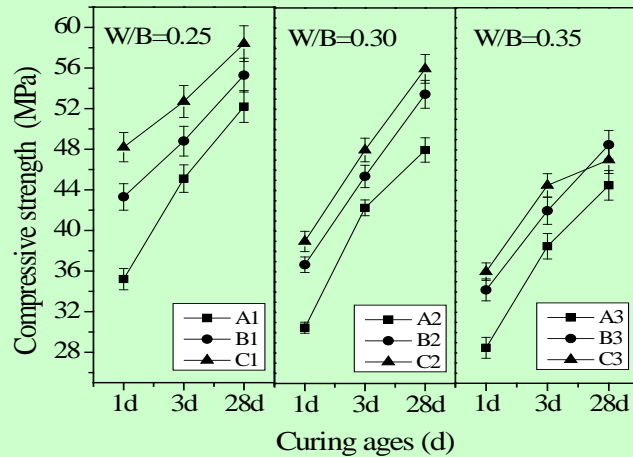
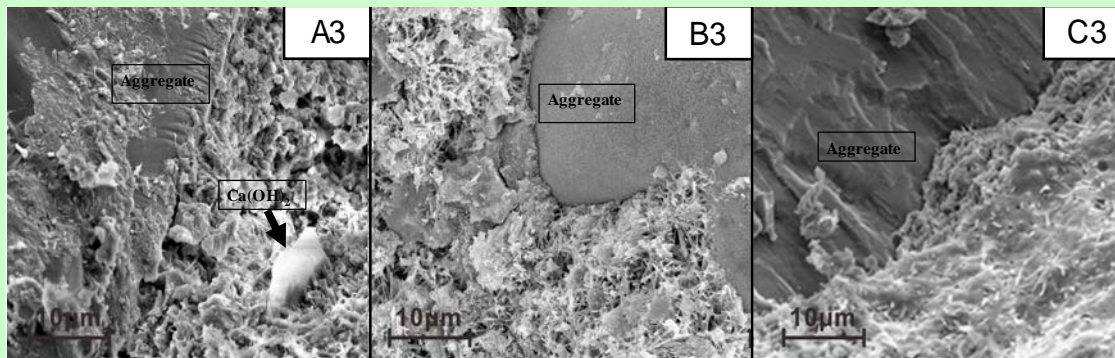


Fig.3 Relationship between pastes thickness on the coated aggregates and compressive strength of HDSCs

Fig.3 shows the compressive strength of HDSC at different water-binder ratios. It can be found that for all three different water-binder ratios, the compressive strength of concrete increased with the increase of paste thickness on the coated aggregates, especially at the early age of 1 and 3 days. Compared with A1, the compressive strength of B1 increased 23%, 8% and 6%, and C1 increased 37%, 17% and 12% at the curing ages of 1, 3 and 28 days respectively. The reason is that the sulphoaluminate cement typically attains high early age strength, which is a result of the cement hydration and increases the interfacial bonds in concrete. Table 4 shows that the cement dosage increased for the same coating thickness.

At a water-binder ratio of 0.30 and 0.35, concrete samples at 28 days attained very similar compressive strengths for aggregates with a coating thickness of $20\mu\text{m}$ and $30\mu\text{m}$. Although the general trend shows the concrete compressive strength increasing with increase of the paste thickness on the coated aggregates, the compressive strength of B2 is close to that of C2 and the compressive strength of B3 is higher than that of C3. The reason can be mainly attributed to the paste thickness on the coated aggregates which improved the structure of the interface transition zone (ITZ) between cement paste and the aggregates. With the decrease of the coating thickness, the space of crystal growth decreases, and the gel could improve the cohesive strength and degree of density [37-38]. The SEM images of concrete A3, B3 and C3 are shown in Fig.4, and it can be seen clearly that the hardened cement paste has plenty of gel (C-S-H gel and $\text{Al}(\text{OH})_3$ gel), fine AFt and little $\text{Ca}(\text{OH})_2$. The hydration of sulphoaluminate

246 cement can produce plenty of gel and AFt in B3, leading to a more compacted ITZ
247 compared with A3 and C3.



248

249

Fig.4 SEM images of interfacial transition zone (ITZ) for HDSCs at 28 days

250

251 **4.2 Electrical resistivity**

252 Several studies [39-40] consider electrical resistivity of concrete is an important
253 factor that indicates the permeability of concrete to aggressive agents such as chloride
254 and carbon dioxide, because electrical resistivity has a strong correlation with the
255 concrete microstructure. The electrical resistivity was decided by the pore solution,
256 which provided a path of conductive ions. This improved conductive performance, and
257 accelerated the corrosion of concrete cubes [41-42].

258 The electrical resistivity results for HDSCs are shown in Fig.5. The electrical
259 resistivity of all the samples increased with the rise of the curing age, particularly at the
260 ages of 1 and 3 days. This can simply be explained by the fact that sulphoaluminate
261 cement has the characteristic of rapid hydration and hardening, and the porosity of
262 hardened cement paste is higher than that of the aggregates. With the increase of paste
263 coating thickness on the coated aggregates, the electrical resistivity of HDSCs
264 decreased at all three water-binder ratios. The electrical resistivity of A1 was 44%,
265 33% and 13% higher than that of C1 at the ages of 1, 3 and 28 days, respectively.
266 Sample A2 was 42%, 35% and 23% higher than that of the sample C2 at the ages of 1d,
267 3 and 28 days, respectively. From Table 4, the dosage of cement increased with the
268 increase of the paste thickness on the coated aggregates. So porosity of concrete
269 relatively increased with the increase of the sulphoaluminate cement dosage at the
270 same water-binder ratio.

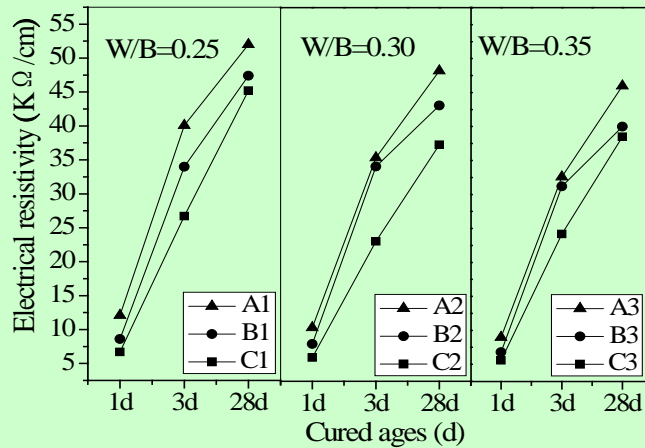
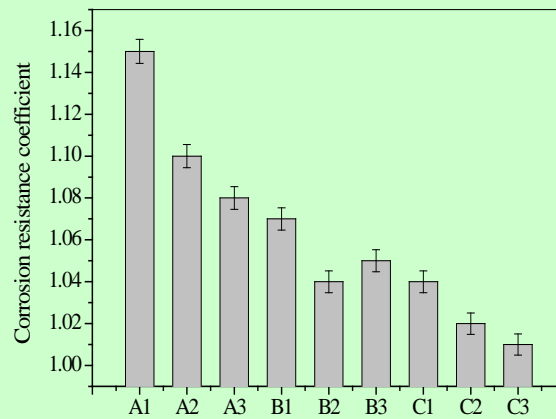


Fig.5 Effect of the paste thickness on the coated aggregates on electrical resistivity of HDSC

4.3 Sulfate attack resistance

The coefficient of sulfate attack resistance is a key parameter in measuring the durability of concrete hence the resistance coefficients of HDSCs were calculated using Equation (2). The coefficients of sulfate attack resistance at the curing age of 28 days are shown in Fig.6. The sulfate attack resistance coefficients of HDSCs were higher than 1.0, which means that the compressive strength of concrete samples cured in the 5% Na₂SO₄ solutions are higher than of those cured in the water at 28 days, indicating that former samples have much better capability of resisting sulfate attack. With the increase of paste thickness on the coated aggregates, the sulfate attack resistance coefficients decreased evidently at the same water-binder ratio. The coefficient of A1 was 10% higher than that of C1, and A3 was 6% higher than that of C3. Sulfate attack resistance is a very important property of concrete and many studies have found that the use of an excessive amount of cement, or too much water, can result in high permeability which has a negative effect on the durability [14, 15, 43]. When the amount of paste thickness on the coated aggregates was appropriate, the structure of concrete could reach up to the close packing. Using too little paste was not enough to fill the voids between the aggregates and too much paste would break the close packing structure, which can be used to explain the reduced sulfate attack resistance of C3. Therefore, the proper dosage of cement can also be used to produce

293 HDSCs with excellent mechanical properties and elevated resistance to sulfate attack.



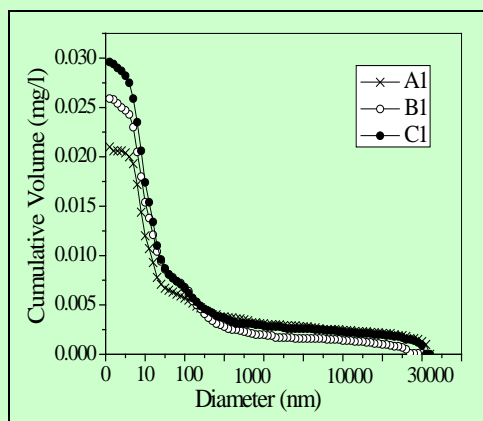
294

295 Fig.6 Sulfate attack resistance of HDSCs at a curing age of 28 days

296

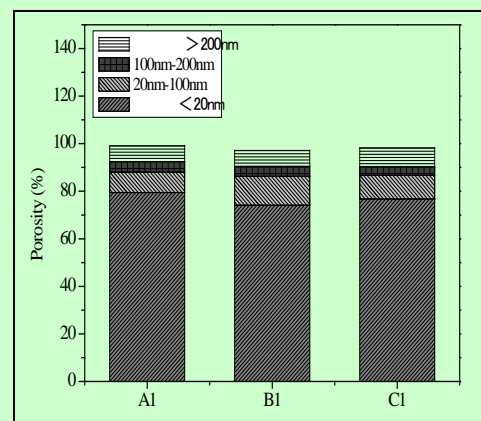
297 **4.4 Pore structure of HDSCs**

298 The pore structure of A1, B1 and C1 at a curing age of 28 days is shown in Figure
 299 7, Figure 8 and Table 5. Figures 7 and 8 showed that the number of micropore (less
 300 than 20nm) and macropore (more than 200nm) was more than 70% and less than 10%
 301 respectively. The cumulative volume of pores in A1 was much more than that in C1,
 302 and the volume of micropore of the former was lower than that of the latter. These pore
 303 structure results are in accordance with the results of electrical resistivity ($t=10\mu m$) in
 304 Fig.5 and sulfate corrosion resistance ($t=10\mu m$) in Fig.6.



305

306 Fig.7 Cumulative pore volume of HDSCs



307 Fig.8 Pore size distribution of HDSCs

308 Table 5 demonstrates that the porosity, pore volume and specific area of the pores
 309 showed an increasing trend with the increase of coating thickness. The average size of
 310 pore was below 12.4nm. Therefore, the structure of HDSCs was very compact.

Table 5 Pore structure characteristic parameters of HDSCs

	Porosity (%)	Pore Volume (<i>ml/g</i>)	Specific Area of Pores (<i>m²/g</i>)	Average Pore Size (<i>nm</i>)
A1	5.0831	0.0210	6.783	12.4
B1	6.1891	0.0259	8.457	12.2
C1	6.9700	0.0296	10.014	11.8

311

312 **5. Conclusion**

313 (1) HDSCs were designed using an improved DMDA method and Fuller curve.
 314 Investigations based on compressive strength, electrical resistivity, sulfate attack and
 315 pore structure analysis indicate that the paste thickness on the coated aggregate is a key
 316 parameter affecting properties of sulphoaluminate cement concrete.

317 (2) The compressive strength of HDSCs increased with the increase of paste
 318 thickness on the coated aggregates, particularly at the early stages of curing, namely 1
 319 and 3 days. When paste thickness on the coated aggregate was $10\mu m$, the compressive
 320 strength increased 23% and 8% compared with $20\mu m$, and increased 37% and 17%
 321 compared with $30\mu m$ at the curing ages of 1 and 3 days, respectively.

322 (3) With the increase of paste thickness on the coated aggregates, the electrical
 323 resistivity of HDSCs decreased at the same water-binder ratio. When the paste
 324 thickness on the coated aggregate was $10\mu m$, the electrical resistivity of HDSC was
 325 44%, 33% and 13% higher than that of sample with $30\mu m$ at the ages of 1, 3 and 28
 326 days, respectively.

327 (4) The sulfate attack resistance coefficients of HDSCs at 28 days were higher
 328 than 1.0, suggesting that concrete samples cured in the 5% Na_2SO_4 solutions have
 329 much better capability of sulfate attack resistance. With the increase of paste thickness
 330 on the coated aggregates, the sulfate attack resistance coefficients decreased evidently.
 331 At the same water-binder ratio, the coefficient of HDSCs with $10\mu m$ was 10% higher
 332 than that of HDSCs with $30\mu m$.

333 (5) At 28 days, the porosity, pore volume and specific pore area of HDSCs showed
 334 an increasing trend with an increasing paste thickness on the coated aggregates. The
 335 porosity of HDSCs was below 7% with 70% micropore ($<20nm$), and the average pore
 336 size was below $12.4nm$.

337

338 **Acknowledge**

339 This work is funded by Natural Science Foundation of China under the grants of
340 51302104 and 5142109, and the Science and Technology Development Plan of
341 Shangdong Province under the grant of 2014GZX208001. In addition, this work is also
342 sponsored by the Program for Science Research Innovation Team in Colleges by
343 Universities of Shangdong Province.

344

345 **Reference**

- 346 [1] Ali M M, Gopal S, Handoo S K. Studies on the formation kinetics of calcium
347 sulphoaluminate. *Cement and concrete research*. 1994; 24(4): 715-720.
- 348 [2] Cheng X, Chang J, Lu L, et al. Study of Ba-bearing sulphoaluminate minerals and
349 cement. *Cement and Concrete Composites*. 2000; 30(1): 71-81.
- 350 [3] Cheng X, Chang J, et al. Study on the Hydration of Ba-bearing calcium
351 sulphoaluminate in the presence of gypsum. *Cement and Concrete Research*. 2004;
352 34(11): 2009-2013.
- 353 [4] Zhou H, Liu J, et al. Hydration kinetics process of low alkalinity sulphoaluminate
354 cement and its thermodynamical properties. *Proc. Eng*. 2012; 27: 323-331.
- 355 [5] Zhao J, Cai G, et al. Influences of freeze–thaw cycle and curing time on chloride
356 ion penetration resistance of sulphoaluminate cement concrete. *Construction and
357 Building Materials*. 2014; 53: 305-311.
- 358 [6] Duan P, Chen W. Influence of layered double hydroxides on microstructure and
359 carbonation resistance of sulphoaluminate cement concrete. *Construction and
360 Building Materials*. 2013; 48: 601-609.
- 361 [7] Yang C C, Lin J D, Chiang H W, et al. Pore Distribution and Durability of Cement
362 Mortar by the Magnetic Resonance Imaging[C]. *Applied Mechanics and Materials*.
363 2015, 764: 132-137.
- 364 [8] Zahedi M, Ramezani pour A A, et al. Evaluation of the mechanical properties and
365 durability of cement mortars containing nanosilica and rice husk ash under
366 chloride ion penetration. *Construction and Building Materials*. 2015; 78: 354-361.

- 367 [9] Hang M, Li H. Pore structure and chloride permeability of concrete containing
368 nano-particles for pavement. *Construction and Building Materials*. 2011; 25(2):
369 608-616.
- 370 [10] Hwang C L, Hsieh S L. The effect of fly ash/slag on the property of reactive
371 powder mortar designed by using Fuller's ideal curve and error function.
372 *Computers and Concrete*. 2007; 4(6): 425-436.
- 373 [11] Hwang C L, Chen C.T. Application of Fuller's ideal curve and error function to
374 making high performance concrete using rice husk ash. *Computers and Concrete*.
375 2012; 10(6): 1123-1126.
- 376 [12] Hwang C L, S.L Lee et al. The study on the densified mixture design method of
377 high performance concrete and its early properties. *Journal of the Chinese*
378 *Hydraulic Engineering*. 1996; 8(2): 207-219.
- 379 [13] Chen Y Y, Tuan B L, et al. Effect of paste amount on the properties of
380 self-consolidating concrete containing fly ash and slag. *Construction and Building*
381 *Materials*. 2013; 47: 340-346.
- 382 [14] Hwang C L, Huynh T P. Investigation into the use of unground rice husk ash to
383 produce eco-friendly construction bricks. *Construction and Building Materials*.
384 2015; 93: 335-341.
- 385 [15] Wang H Y, Tsai K C. Engineering properties of lightweight aggregate concrete
386 made from dredged silt. *Cement and Concrete Composites*. 2006; 28(5): 481-485.
- 387 [16] Chang P K. An approach to optimizing mix design for properties of
388 high-performance concrete. *Cement and Concrete Research*. 2004; 34(4): 623-629.
- 389 [17] Felekog̃lu B, Türkel S, Baradan B. Effect of water/cement ratio on the fresh and
390 hardened properties of self-compacting concrete. *Building Environment*. 2007;
391 42(4): 1795-802.
- 392 [18] Aitcin P C. The durability characteristics of high performance concrete: a review.
393 *Cement and Concrete Composites*. 2003; 25(4-5): 409-20.
- 394 [19] Wang H Y, Hwang C L. An approach of using ideal grading curve and coating
395 paste thickness to evaluate the performances of concrete-(1): Theory and
396 formulation. *Computers and concrete*. 2012; 10(10): 19-33.

- 397 [20] Okundi E, Buenfeld N R, et al. Effect of cement content on transport in concrete.
398 Magazine of Concrete Research, 1998, 50(4):339-351.
- 399 [21] Hwang C L, Lee S L, Lin F Y, et al. Densified mix design algorithm and early
400 properties of HPC. J. Chin. Inst. Civil Hydraul. Eng, 1994; 8(2): 217-219.
- 401 [22] Koliass S, Georgiou C. The effect of paste volume and of water content on the
402 strength and water absorption of concrete. Cement and Concrete Composites. 2005;
403 27(2): 211-216.
- 404 [23] Chen Y, Wei J, Li F, et al. Effect of the paste coating layer and mortar coating
405 layer on the properties of fresh self-compacting concrete. Journal of Sustainable
406 Cement-Based Materials, 2015; 4(3): 194-204.
- 407 [24] Sobolev K, Amirjanov A. Application of genetic algorithm for modeling of dense
408 packing of concrete aggregates. Construction and Building Materials. 2010; 24(8):
409 1449-1455.
- 410 [25] Gonzalez C, Etxeberria M. Properties of high performance concrete made with
411 recycled fine ceramic and coarse mixed aggregates. Construction and Building
412 Materials. 2014; 68: 618-626.
- 413 [26] Elrahman M A, Hillemeier B. Combined effect of fine fly ash and packing density
414 on the properties of high performance concrete: An experimental approach.
415 Construction and Building Materials. 2014; 58: 225-233.
- 416 [27] Bai W, Zhang J. Proportion design of polymeric cement concrete based on
417 volumetric analysis. Applied Mechanics and Materials. 2014; 584: 1809-1813.
- 418 [28] García-Taengua E, Sonebi M, Crossett P, et al. Performance of sustainable SCC
419 mixes with mineral additions for use in precast concrete industry. Journal of
420 Sustainable Cement-Based Materials. 2015; 1-19.
- 421 [29] Zhang J, Wang S, Lu L. Effect of aggregate gradation with Fuller distribution on
422 properties of sulphoaluminate cement concrete. Journal of Wuhan University of
423 Technology-Mater. 2015; 30(5): 1029-1035.
- 424 [30] GB/T50080-2002. Standard for test method of performance on ordinary fresh
425 concrete. Beijing: Standardization Administration of the People's Republic of
426 China; 2002.

- 427 [31] GB/T 50081-2002. Standard for test method of mechanical properties on ordinary
428 concrete. Beijing: Standardization Administration of the People's Republic of
429 China; 2002.
- 430 [32] GB/T 50082-2009. Standard for test method of long-term performance and
431 durability of ordinary concrete. Beijing: Standardization Administration of the
432 People's Republic of China; 2009.
- 433 [33] Hüsken G, Brouwers H J H. A new mix design concept for earth-moist concrete: A
434 theoretical and experimental study. *Cement and Concrete Research*. 2008; 38(10):
435 1246-1259.
- 436 [34] W B Fuller, S E Thompson. The laws of proportioning concrete. *J. Transp. Eng.-*
437 *ASCE*. *Cement and Concrete Composites* 1907; 59: 67-143.
- 438 [35] Cai Z, Huang Z et al. New approach to design concrete mix proportions by
439 coating thickness of aggregates. *Journal of Building Materials*. 2009; 12(4):
440 152-157.
- 441 [36] Zhang J, Huang Z et al. Effects of paste thickness on coated aggregates on
442 properties of concrete. *Journal of Building Materials*. 2009; 12(4): 384-427.
- 443 [37] Nili M, Ehsani A. Investigating the effect of the cement paste and transition zone
444 on strength development of concrete containing nanosilica and silica fume.
445 *Materials & Design*. 2015; 75: 174-183.
- 446 [38] Poon C S, Shui Z H, Lam L. Effect of microstructure of ITZ on compressive
447 strength of concrete prepared with recycled aggregates. *Construction and Building*
448 *Materials*. 2004; 18(6): 461-468.
- 449 [39] Medeiros-Junior R A, Lima M G. Electrical resistivity of unsaturated concrete
450 using different types of cement. *Construction and Building Materials*, 2016;
451 107(15): 11-16.
- 452 [40] Ghods P, Isgor O B, Pour-Ghaz M. A practical method for calculating the
453 corrosion rate of uniformly depassivated reinforcing bars in concrete. *Materials*
454 *and Corrosion*. 2007; 58(4): 265-272.
- 455 [41] Liu Z, Zhang Y, Jiang Q. Continuous tracking of the relationship between
456 resistivity and pore structure of cement pastes. *Construction and Building*

457 Materials. 2014; 53(28): 26-31.

458 [42] Wang Z, Zeng Q, Wang L, et al. Characterizing blended cement pastes under
459 cyclic freeze–thaw actions by electrical resistivity. Construction and Building
460 Materials. 2013; 44: 477-486.

461 [43] Su N, Hsu K C, Chai H W. A simple mix design method for self-compacting
462 concrete. Cement and Concrete Research, 2001; 31(12): 1799-1807.